Kochi Chapter

Indian Geotechnical Conference
IGC 2022
15th – 17th December, 2022, Kochi

An Effective Frequency Filtering Approach to Improve GPR Data Resolution under the Concrete Pavements

Prabhakar Vishwakarma[1], Silky Agrawal[2] and Amit Prashant[3]

[1] Research Scholar, Discipline of Civil Engineering, IIT Gandhinagar, 382055
E-mail: prabhakar.18350004@iitgn.ac.in
[2] Founder, GeoCarte Radar Technology Pvt. Ltd., IIT Gandhinagar, 382055
[3] Professor, Discipline of Civil Engineering, IIT Gandhinagar, 382055

Abstract. This study focuses on developing the advanced analysis procedure for increasing the underground utility resolution using the RADAN software. The chop-off of the time domain signal and frequency band filtering approach are adopted to improve underground utility resolution. The rebars of rigid pavement symbolically appear in the form of hyperbolic rings as an output of the GPR data. These small hyperbolic rings reduce the resolution of underground utilities, and further difficulty arises in identifying the appropriate location of underground utilities. Therefore, the resolution of underground utilities is compared with the proposed processing steps of frequency band filtering with the incremental and constant time chop-off approach. The incremental time chop-off approach results in a high resolution of underground utilities compared to the constant time chop-off approach in the GPRs output. The performance of the proposed processing steps is explored with the six different earth profiles. The findings of this study demonstrate that (1) GPR data collected using a 900 MHz antenna is highly sensitive and removing the RADAN spectrum of rebars zone is an effective way for utility detection of depth less than 1m, and (2) High rebars resolution is obtained using 900 MHz compared to 400 MHz.

Keywords: GPR; Underground utility; hyperbolic rings; Frequency band filtering; Chop-off.

1 Introduction

In several areas of civil engineering, ground-penetrating radar (GPR) surveys are adopted to find subsurface utilities. Different frequency bands of electromagnetic waves are emitted into the ground by transmitters, and then the reflected waves are picked up by receivers. The gathered signals can be used to pinpoint the exact position of the subsurface abnormality. GPR has been used to describe the infill, groundmass, soil hydraulic characteristics, and soil cracks (Serzu et al., 2004). The location and identification of underground utilities (Jaw and Hashim, 2013; Ni et al., 2010), the detection of voids and sinkholes (Sevil et al., 2017), the determination of soil water content (Schwartz et al., 2009), the assessment of the ground structure around tunnels and linings (Porsani et al., 2012), and the inspection of road pavement are other common uses (Shangguan et al., 2016; Zhao and Al-Qadi, 2016). GPR is now well known for finding subsurface cavities under the pavement.

The irregularity in the pavement surface is caused by the settlement in the soil layer beneath the pavements. One cause of these kinds of unforeseen settlements is the leaking of liquid from underground pipes. Kim and Park (2018) studied the damages caused by the subsidence of roads in suburban areas and the sudden sinking of buildings. Expanded polystyrene (EPS) was used to create fake voids beneath the asphalt pavement, and the signals from impulse and step-frequency type GPR were compared to determine which was the most effective technique for finding cavities (Kim et al.,1967). In the meantime, a model chamber from the GPR testing was used to identify the depth and position of buried objects (Lee, 2016). Additionally, a tool for image processing was created to aid in the analysis of the GPR survey data.

Similar to this, using the GPR survey data, cavities were found using an image processing technique (Kim et al., 2017). Furthermore, in another study, 3D-GPR measurements were used to determine the relative permittivity of the ground on test beds and actual roads (Jang, 2019). When evaluating GPR signals, it has been discovered that it is advantageous to use the collected longitudinal, transverse, and depth images all at once. The development of the literature on the use of GPR surveys to identify utilities in various types of pavement is discussed chronologically (Table 1). Due to electromagnetic wave scattering, a steel bar in the stiff pavement reduces the resolution of underground utilities. However, the study to improve utility resolution when steel bars are present is unaffected. Therefore, the development of a reliable method to increase the utility resolution in GPR survey is the main focus of this study. To improve the resolution of subsurface utilities, we introduced a frequency band filtering strategy and time domain signal chop-off techniques. The summary of literature evolved on the utility detection beneath the pavements are presented in Table-1.

Table 1. Literature summary for the utility detection under the pavement.

Author and Year	Objective	Antenna used	Findings of study
Maser et al. (1991)	To determine the contact between the asphalt and base layers	1 GHz horn antenna	Asphalt thickness of 25 to 250 mm
Saarenketo et al. (1997)	To assess the material density for quality control	1 GHz	Measurement of dielectric constant of pavement
Hugenschmidt et al. (1998)	To detect the contact between new and old pavement surface	2.5 GHz 900 MHz	Detection of damaged zone
Al-Quadi et al. (2005)	To identify the metal bar and layer thickness	1.5 GHz	Rebar cover depth estimation
Gui et al. (2016)	Automated defect detection and robotic runway	1 GHz	Pavement quality and different type of defect
Zhang et al. (2020)	Moisture detection in asphalt pavement	2.3 GHz	Hyperbolic curve for buried object
Rhee et al. (2021)	An expressway investigation	400 MHz	Energy attenuation due to rebar scattering
Xie et al. (2021)	To identify pavement diseases in GPR post processing	200 MHz	Interpretation standards are developed

2 Background

2.1 Principle of GPR

The most popular GPR antennas available at frequencies of 200 MHz, 400 MHz, and 900 MHz, respectively. The 200 MHz, 400 MHz, and 900 MHz antenna are used to investigate depths of 6 m, 3 m, and 1 m, respectively. The electromagnetic pulse beamer is produced by the transmitter antenna, as depicted in Fig. 1a, and the receiver receives the reflected signal via a circuit inside the radar control unit. Depending on the dielectric constant of the material (air/pavement layer, ground/cavity or utility, etc.), some electromagnetic wave is transmitted and some is reflected through the subsurface medium. In order to process the data of the pavement's subsurface, numerous side-by-side scans are acquired when GPR antennas run along the survey line. Eq. 1 and Eq. 2 present the incident electromagnetic waves at the place of reflection.

$$E_i(z,t) = E_i\, e^{j\,(k_1 z - \omega t)} x \tag{1}$$

$$B_i(z,t) = \frac{E_i}{v_1}\, e^{j\,(k_1 z - \omega t)} y \tag{2}$$

The reflected electromagnetic fields are expressed in Eq. 3 and Eq. 4.

$$E_r(z,t) = E_r e^{j\,(-k_1 z - \omega t)} x \tag{3}$$

$$B_r(z,t) = -\frac{E_r}{v_1} e^{j\,(-k_1 z - \omega t)} y \tag{4}$$

where $E_i(z,\ t)$ and $B_i(z,\ t)$ indicate the incident electric and magnetic fields at a specific depth z and point in time t. $E_r(z,\ t)$ and $B_r(z,\ t)$ indicate the reflected electric and magnetic fields at a specific depth z and point in time t. E_i is the amplitude of the incident electric field. E_r represents the amplitude of the reflected electric field, which is function of refractive indices of medium and given in Eq. 5. k_1, ω, and v_1 refer to the wavenumber, frequency, and velocity of the electromagnetic waves in the corresponding medium, respectively.

$$\frac{E_r}{} = \frac{n_1 - n_2}{n_1 - n_2} \frac{E_i}{} = \frac{\sqrt{\varepsilon_1 \mu_1} - \sqrt{\varepsilon_2 \mu_2}}{\sqrt{\varepsilon_1 \mu_1} + \sqrt{\varepsilon_2 \mu_2}} E_i \tag{5}$$

where n_1 and n_2 are the refractive indices of each medium. ε_1 and ε_2 are relative permittivity. μ_1 and μ_2 are relative permeability of two soil mediums.

2.2 Background filtering to enhance underground utility visualization

To extract the reflected signals from underground objects from the GPR data, it is necessary to remove the undesired background signals, including (1) pavement surface reflections, (2) reflections from underground layers, and (3) background noise. Interactions between the electromagnetic waves and buried objects are identified more easily

by representing the measured time-domain signal s ($T \times 1$ vector) as a weighted linear combination of bases with the following transformation (Yoon et al., 2016):

$$s = D\alpha,\ D = \{d_1, d_2, \quad , d_L\} \tag{6}$$

Where, T is the maximum duration of measured time-domain signal, α is a representation of s in the transformed domain with the dimension $L \times 1$. D is a $T \times L$ dictionary matrix and consists of d_i bases ($i = 1, \ldots, L$). Each basis d_i is a time-domain signal with the same dimensions as s. We defined a reference point as a pristine scanning location without underground objects in the inspection area. The reference signal E_{ref} measured from the reference point, which is expressed using Eq. 7.

$$E_{ref}(t) = E\, e^{-j\omega t} \tag{7}$$

Each basis represents a reference signal with a specific time delay in this study. For example, d_i is reference signal with a time delay of $(\frac{L}{2} - 1)\,\Delta t$:

$$d_i = E\,(t + (\tfrac{L}{2} - 1)\,\Delta t) = E\,(t + (L - 1)\,\Delta t) = E\, e^{-j\omega(t + (L^F - 1)\Delta t)} \tag{8}$$

In other words, the measured GPR data s is represented as a sum of reference signals with different time delay. Any change in s from E_{ref}, such as underground object reflections, is compensated by adding weighted d_i with proper time delay.

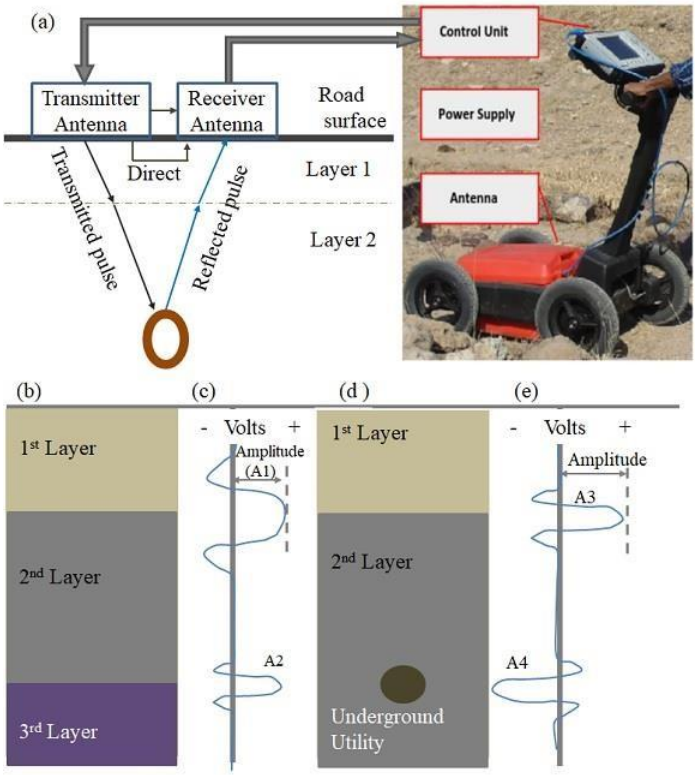

Fig. 1. (a) Illustration of GPR scanning on the road with the travel of electromagnetic waves and RADAN setup; (b) Typical soil layer without underground utility; (c) GPR waveform in absence of underground utility; (d) Typical soil layers with underground utility; (e) GPR waveform in the presence of underground utility.

3 Method

The GPR waveforms in the presence and absence of underground utility are discussed by the examples. Fig. 1b depicts a typical soil layer without subsurface utilities, and it's electromagnetic waveform is observed with the same amplitude polarity A1 and A2, as shown in Fig. 1c. The presence of an underground utility in a typical soil layer (Fig. 1d) alters the amplitude polarity of the electromagnetic waveform from A3 to A4, as illustrated in Fig. 1e. Dowel bars are found in various locations in the rigid pavements. In the GPR processed data, the existence of these bars is depicted as a hyperbolic ring. The observed behavior of the electromagnetic waves are pointed out as follows:

1) Multiple reflections from the dowel bar in the concrete
2) Significant abruption of electromagnetic wave transmission
3) Hyperbolic ring decreases the resolution of utility due to the multiple reflection and refraction (Fig. 2)

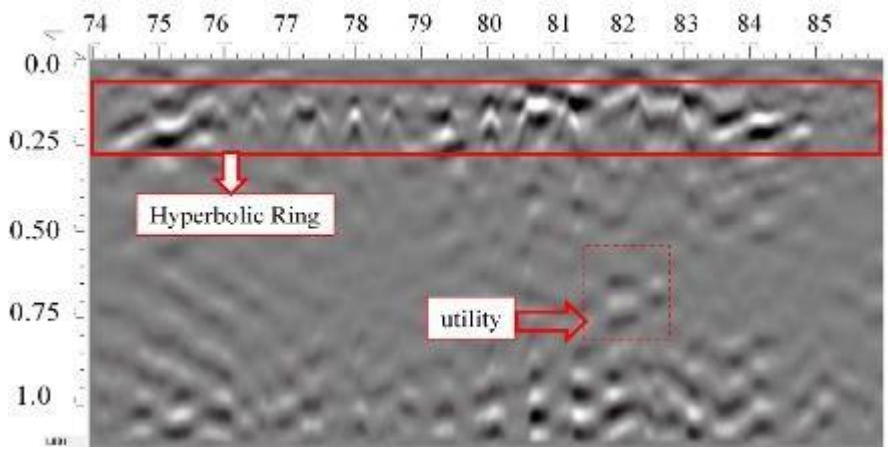

Fig. 2**.** Utility resolution effect due to steel bar in the rigid pavement using GPR survey (900 MHz).

Using the 400 MHz (50 ns) and 900 MHz (20 ns) antennas, a GPR survey is carried out in the distance mode. Utilizing the time zero correction, background removal, frequency deconvolution, and range gain filtering techniques, collected data is processed using RADAN software.

The frequency and wave propagation time of the transmitter and receiver antenna are calculated during the time zero correction operation. Additionally, for each GPR trace data, the zero amplitude value of the signal is eliminated and interpolated.

In the continuation of GPR processing, background elimination is one of standard step. The average trace subtraction approaches and modified variations, like moving average trace subtraction, are also applied for reducing the background noise (Yoon et al., 2016).

A guideline for selecting a narrow frequency range is provided by the time-frequency window of the RADAN software of a GPR record, and the deconvolution aims to contrast signals to increase resolution. The goal is to exclude the source wavelet's

influence from the GPR data and preserve the surface layers' impulse response. The horizontal layering, homogeneous intra-layer velocity, and coherent signal reflection at the interface are all presumptions made by this deconvolution procedure (Maruddani and Sandi, 2019).

A finite impulse response (FIR) band pass filter (Xie et al., 2013) filters the time window signal using the moving window approach based a finite unit impulse response. The FIR expresses the input and output data, as given in the Eq. 9.

$$y(n) - \sum_{m=0}^{N-1} h(m)\, x(n-m) \tag{9}$$

Here $y(n)$ and $x(n)$ represent the output and input data, respectively. The unit impulse response $h(m)$ is finite, and we took advantage of the ideal filter response function $H_d(e^{j\omega})$ and window function $\omega(m)$ to get it:

$$H(z) = \sum_{m=0}^{M-1} h(m)\ z^{-m} \tag{10}$$

$$h_d(m) = \frac{1}{2\pi} \int_{-\pi}^{\pi} H_d(e^{j\omega})\ e^{j\omega}\, d\omega \tag{11}$$

$$h(m) = \omega(m)\ h_d(m) \tag{12}$$

4 GPR processing Results

The GPR data collected from 400 MHz and 900 MHz antennae are processed by adopting the processing steps which are discussed in the section 3.0. Time chop off, and frequency band pass filter are additionally applied in the RADAN software framework.

4.1 Incremental time chop off with frequency band pass filter

The summary of the processing steps with the corrected depth along with the frequency band pass filter are shown in Table-2 and Table-3. The GPR data were collected using 400 MHz (as shown in Table-2) and 900 MHz antennae (as shown in Table-3). The limits of high and low pass filters are varied by 50 MHz and RADAN data is chopped off by applying time correction, which removes the RADAN spectrum of the reinforced zone. As the chopping off of RADAN data is done, the resolution of underground utility increases, as shown in Fig. 3 and Fig. 4.

4.2 Constant time chop off with frequency band pass filter

Table-4 and Table-5 present the corrected depth along with the frequency band pass filter for the GPR data collected using 400 MHz and 900 MHz antennae, respectively. The limit of the high pass filter is increased while the low pass filter is decreased with the constant chop-off in the time window, which only removes the RADAN spectrum of the reinforced zone. The utility resolution is significantly improved by narrowing the frequency band filtering, as shown in Fig. 5 and Fig. 6.

Table 2**.** Time and Depth correction along with frequency band filtering for 400 MHz antennae in Profile 1 and 2.

Processing Steps	Time zero correction (ns)	Depth correction (m)	Vertical low filter (MHz)	Vertical high pass filter (MHz)
1	0	0	650	62
2	-12	0.6m	500	80
3	-24	0.9m	400	80
4	-36	1.2m	550	70

Table 3**.** Time and Depth correction along with frequency band filtering for 900 MHz antennae in Profile 3 and 4.

Processing Steps	Time zero correction (ns)	Depth correction (m)	Vertical low filter (MHz)	Vertical high pass filter (MHz)
1	0	0	1200	100
2	-5	0.25m	1150	132
3	-10	0.5m	1000	111

5 Discussion

The underground utility resolutions obtained from the proposed processing steps of frequency band filtering in incremental and constant time chop-off are compared. The incremental time chop-off produces a high resolution of GPR data as compared to constant time chop-off processing steps. The 900 MHz antenna provided the utility mapping at shallower depth as compared to the 400 MHz antenna for the same soil condition, as shown in Fig. 3 and Fig. 4. However, these processing steps are highly susceptible to noise and small signal disturbances in the time domain, e.g., variations in pavement thickness, type of rebars, and utilities below the pavement. Therefore, the addition of proposed processing steps in the GPR conventional processing steps provided the better resolution of underground utility beneath the pavements.

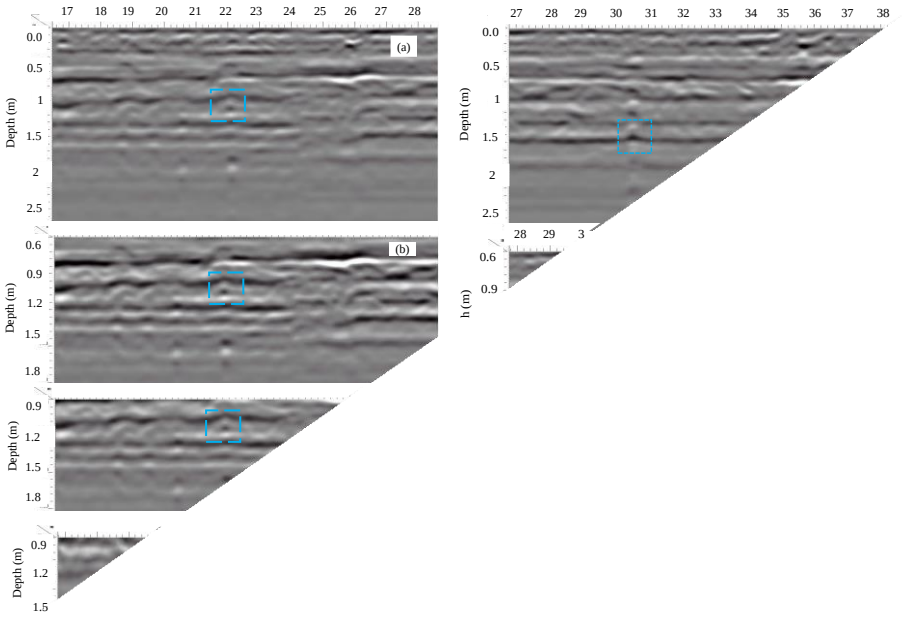

Fig. 3. 400 MHz antenna GPR survey to enhance the utility resolution located at 1m for Profile-1 applying the correction of (a) time zero; (b) 0.6m; (c) top chop-off at 0.9m (initial depth) and (d) bottom chop-off at 1.5m (Table 2). The utility resolution enhancement located at 1.5 m for Profile-2 applying the correction of (e) time zero; (f) 0.6m; (g) 0.9m and (h) 1.2m (Table 2)

Table 4. Time-depth correction with frequency band filtering of 400 MHz antenna in Profile 5.

Processing Steps	Time zero correction (ns)	Depth correction (m)	Vertical low filter (MHz)	Vertical high pass filter (MHz)
1	0	0	800	100
2	-5	0.25	600	120
3	----	-----	500	140
4	-----	-----	450	150

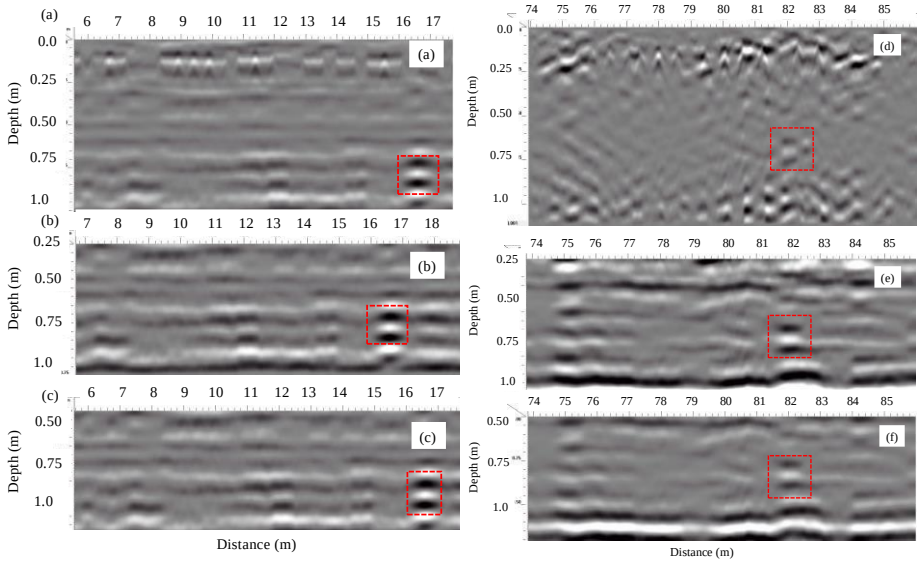

Fig. 4. 900 MHz antenna GPR survey to enhance the utility resolution located at 0.8 m for Profile-3 applying the correction of (a) time zero; (b) 0.25m; (c) 0.5m (Table 3)**.** Enhancement of utility resolution located at 0.75 m for Profile-4 applying the correction of (d) time zero; (e) 0.25m; (f) 0.5m (Table 3)

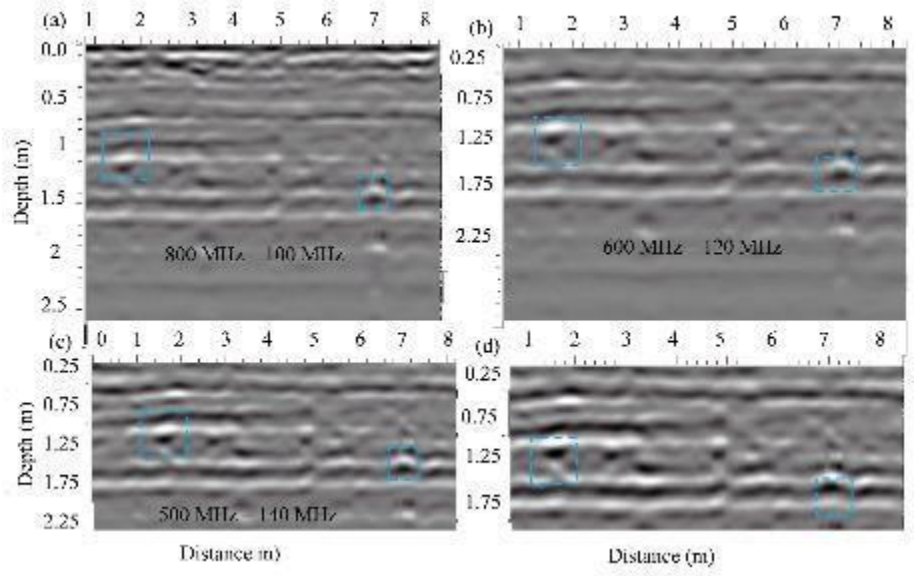

Fig. 5. 400 MHz antenna GPR survey to enhance the utility resolution located at 1.25m and 1.5m for Profile-5 applying the time zero correction for frequency range of (a) 800-100 MHz; (b) 600-120 MHz, (c) 500-140 MHz , and (d) 450-150 MHz as per Table-4

Table 5. Time and Depth correction along with frequency band filtering for 900 MHz antenna in Profile 6.

Processing Steps	Time zero correction (ns)	Depth correction (m)	Vertical low filter (MHz)	Vertical high pass filter (MHz)
1	0	0	1240	140
2	-5	0.25	1100	250
3	----	-----	1000	300
4	-----	-----	900	350

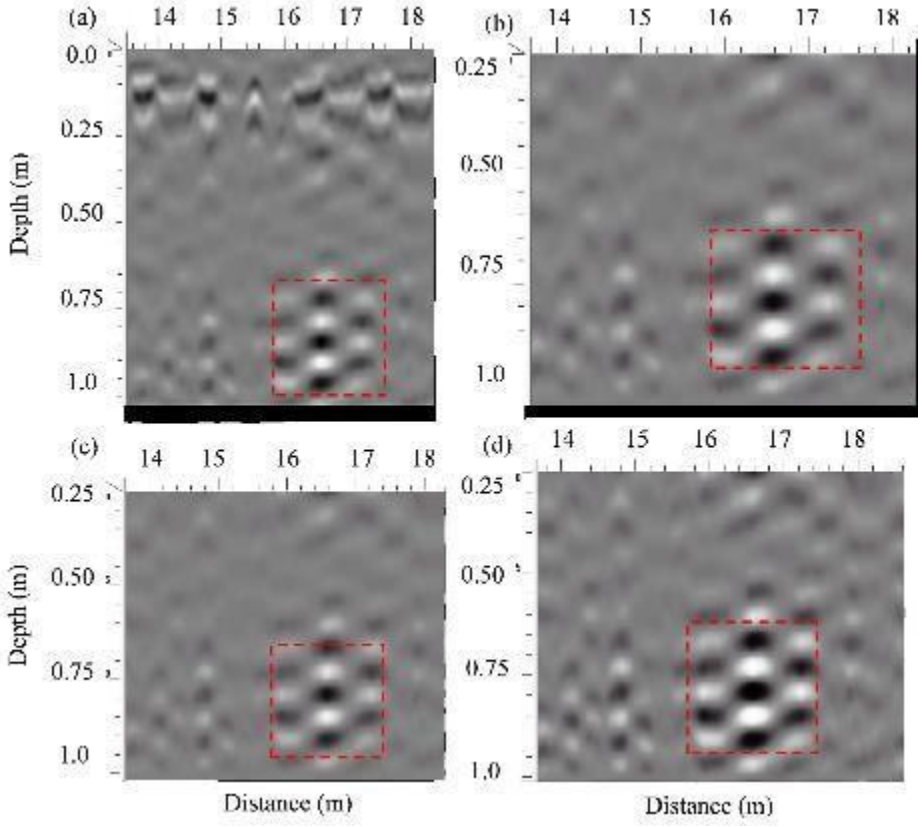

Fig. 6. 900 MHz antenna GPR survey to enhance the utility resolution located at 0.85m for Profile-6 after applying the time zero correction for frequency range of (a) 1240-140 MHz; (b) 1100-250 MHz, (c) 1000-300 MHz and (d) 900-350 MHz, as per Table-5

6 Conclusions

This study proposed a processing step based on time chop-off and frequency band pass filter to enhance the resolution of utility below the rigid pavement. The proposed technique enhances the visibility of subsurface utility (such as, underground pipe, plastic cables etc.) by applying incremental and constant time chop-off along with frequency band pass filtering to the GPR data. The dielectric constant is kept constant for all surveyed profiles using 400 MHz and 900 MHz antennae. It is recommended to classify the underground object based on the contrast of the profile obtained from the GPR survey. However, localization of existing utility detected successfully. The buried objects was successfully detected using the proposed processing steps. The significant finding of this study is given as follows:

1. GPR data collected using a 900 MHz antenna was found to be highly sensitive due to the existence of rebar. Therefore, removal of RADAN spectrum of rebar zone was effective way for utility detection of depth less than 1m.
2. High rebar resolution was obtained using 900 MHz as compared to 400 MHz antennae.
3. The incremental time chop-off and the frequency band pass filtering approach enhanced the resolution of underground utility in the presence of rebar as compared to constant time chop-off. Although, both the processing steps had shown the better resolution over the conventional processing steps.

References

1. Jang, S.L.I., 2019. A Study on the Underground Condition of Road Using 3D-GPR Exploration 20, 49–58
2. Jaw, S.W., Hashim, M., 2013. Locational accuracy of underground utility mapping using ground penetrating radar. Tunn. Undergr. Sp. Technol. 35, 20–29. https://doi.org/10.1016/j.tust.2012.11.007.
3. Kim, Y.T.; Choi, J.Y.; Kim, K.D.; Park, H.M., 1967. A Study on the Selection of GPR Type Suitable for Road Cavity Detection. Angew. Chemie Int. Ed. 6(11), 951–952. 13, 15–38
4. Kim, B., Seol, S.J., Byun, J., 2017. Application of Image Processing Techniques to GPR Data for the Reliability Improvement in Subsurface Void Analysis. Geophys. Geophys. Explor. 20, 61–71.
5. Kim, Y., Park, S.-W., 2018. DEM Simulation on the Initiation and Development of Road Subsidence 33, 43–53.
6. Lee, H.-H., 2016. Image Processing of GPR Detection Data. J. Korea Inst. Struct. Maint. Insp. 20, 104–110. https://doi.org/10.11112/jksmi.2016.20.4.104
7. Maruddani, B., Sandi, E., 2019. The development of ground penetrating radar (GPR) data processing. Int. J. Mach. Learn. Comput. 9, 768–773. https://doi.org/10.18178/ijmlc.2019.9.6.871
8. Ni, S.H., Huang, Y.H., Lo, K.F., Lin, D.C., 2010. Buried pipe detection by ground penetrating radar using the discrete wavelet transform. Comput. Geotech. 37, 440–448. https://doi.org/10.1016/j.compgeo.2010.01.003
9. Porsani, J.L., Ruy, Y.B., Ramos, F.P., Yamanouth, G.R.B., 2012. GPR applied to mapping utilities along the route of the Line 4 (yellow) subway tunnel construction in São Paulo City, Brazil. J. Appl. Geophys. 80, 25–31. https://doi.org/10.1016/j.jappgeo.2012.01.001

10. Rhee, J.Y., Park, K.T., Cho, J.W., Lee, S.Y., 2021. A study of the application and the limitations of gpr investigation on underground survey of the Korean expressways. Remote Sens. 13. https://doi.org/10.3390/rs13091805
11. Schwartz, R.C., Evett, S.R., Bell, J.M., 2009. Complex Permittivity Model for Time Domain Reflectometry Soil Water Content Sensing: II. Calibration. Soil Sci. Soc. Am. J. 73, 898–909. https://doi.org/10.2136/sssaj2008.0195
12. Serzu, M.H., Kozak, E.T., Lodha, G.S., Everitt, R.A., Woodcock, D.R., 2004. Use of borehole radar techniques to characterize fractured granitic bedrock at AECL's Underground Research Laboratory. J. Appl. Geophys. 55, 137–150. https://doi.org/10.1016/j.jappgeo.2003.06.012
13. Sevil, J., Gutiérrez, F., Zarroca, M., Desir, G., Carbonel, D., Guerrero, J., Linares, R., Roqué, C., Fabregat, I., 2017. Sinkhole investigation in an urban area by trenching in combination with GPR, ERT and high-precision leveling. Mantled evaporite karst of Zaragoza city, NE Spain. Eng. Geol. 231, 9–20. https://doi.org/10.1016/j.enggeo.2017.10.009
14. Shangguan, P., Al-Qadi, I., Coenen, A., Zhao, S., 2016. Algorithm development for the application of ground-penetrating radar on asphalt pavement compaction monitoring. Int. J. Pavement Eng. 17, 189–200. https://doi.org/10.1080/10298436.2014.973027
15. Xie, X., Zeng, C., Wang, Z., 2013. GPR signal enhancement using band-pass and K-L filtering: A case study for the evaluation of grout in a shielded tunnel. J. Geophys. Eng. 10, 1–10. https://doi.org/10.1088/1742-2132/10/3/034003
16. Yoon, J.-S., Baek, J., Choi, Y.W., Choi, H., Lee, C.M., 2016. Signal Pattern Analysis of Ground Penetrating Radar for Detecting Road Cavities 7159, 61–67.
17. Zhao, S., Al-Qadi, I.L., 2016. Development of an analytic approach utilizing the extended common midpoint method to estimate asphalt pavement thickness with 3-D ground-penetrating radar. NDT E Int. 78, 29–36. https://doi.org/10.1016/j.ndteint.2015.11.005